Tissue Eng Regen Med (2018) 15(6):735–750
https://doi.org/10.1007/s13770-018-0140-z

Online ISSN 2212-5469
Print ISSN 1738-2696

ORIGINAL ARTICLE

A Comparison of the Effects of Silica and Hydroxyapatite Nanoparticles on Poly(ε-caprolactone)-Poly(ethylene glycol)-Poly(ε-caprolactone)/Chitosan Nanofibrous Scaffolds for Bone Tissue Engineering

Vahideh Raeisdasteh Hokmabad[1] · Soodabeh Davaran[2] · Marziyeh Aghazadeh[3,4] · Effat Alizadeh[3,5] · Roya Salehi[2] · Ali Ramazani[1]

Received: 15 February 2018 / Revised: 26 June 2018 / Accepted: 27 June 2018 / Published online: 14 August 2018

Abstract

BACKGROUND: The major challenge of tissue engineering is to develop constructions with suitable properties which would mimic the natural extracellular matrix to induce the proliferation and differentiation of cells. Poly(ε-caprolactone)-poly(ethylene glycol)-poly(ε-caprolactone) (PCL-PEG-PCL, PCEC), chitosan (CS), nano-silica (n-SiO_2) and nano-hydroxyapatite (n-HA) are biomaterials successfully applied for the preparation of 3D structures appropriate for tissue engineering.

METHODS: We evaluated the effect of n-HA and n-SiO_2 incorporated PCEC-CS nanofibers on physical properties and osteogenic differentiation of human dental pulp stem cells (hDPSCs). Fourier transform infrared spectroscopy, field emission scanning electron microscope, transmission electron microscope, thermogravimetric analysis, contact angle and mechanical test were applied to evaluate the physicochemical properties of nanofibers. Cell adhesion and proliferation of hDPSCs and their osteoblastic differentiation on nanofibers were assessed using MTT assay, DAPI staining, alizarin red S staining, and QRT-PCR assay.

RESULTS: All the samples demonstrated bead-less morphologies with an average diameter in the range of 190–260 nm. The mechanical test studies showed that scaffolds incorporated with n-HA had a higher tensile strength than ones incorporated with n-SiO_2. While the hydrophilicity of n-SiO_2 incorporated PCEC-CS nanofibers was higher than that of samples enriched with n-HA. Cell adhesion and proliferation studies showed that n-HA incorporated nanofibers were slightly superior to n-SiO_2 incorporated ones. Alizarin red S staining and QRT-PCR analysis confirmed the osteogenic differentiation of hDPSCs on PCEC-CS nanofibers incorporated with n-HA and n-SiO_2.

CONCLUSION: Compared to other groups, PCEC-CS nanofibers incorporated with 15 wt% n-HA were able to support more cell adhesion and differentiation, thus are better candidates for bone tissue engineering applications.

Keywords Tissue engineering · Nano-silica · Nano-hydroxyapatite · Human dental pulp stem cells · Nanofibers

✉ Roya Salehi
salehiro@tbzmed.ac.ir

✉ Ali Ramazani
aliramazani@gmail.com; aliramazani@znu.ac.ir

[1] Department of Chemistry, University of Zanjan, P.O. Box 45195-313, Zanjan, Iran

[2] Drug Applied Research Center and Department of Medical Nanotechnology, Faculty of Advanced Medical Science, Tabriz University of Medical Sciences, Tabriz 51666-14733, Iran

[3] Stem Cell Research Center, Tabriz University of Medical Sciences, Tabriz 51666-14733, Iran

[4] Oral Medicine Department of Dental Faculty, Tabriz University of Medical Sciences, Tabriz 51666-14733, Iran

[5] Department of Medical Biotechnology, Faculty of Advanced Medical Science, Tabriz University of Medical Sciences, Tabriz 51666-14733, Iran

1 Introduction

Bone injuries and defects caused by tumor resection, trauma, and congenital deformity remain a major challenge in clinical therapy [1]. Compared to present-day clinical therapies such as autografts and allografts [2], bone tissue engineering provides an alternative approach for bone reconstruction through the substitution of damaged tissues and has developed rapidly [3–7]. Over the past years, nanoscale substrates have attracted increasing attention in bone tissue engineering because they can affect cell performance, such as migration, proliferation, mitosis and lineage-specific differentiation, and extracellular matrix (ECM) deposition [8, 9]. In the nano-matrix realm, the 3-D nanofibrous scaffolds have been extensively utilized in tissue regeneration applications [10, 11]. Besides the narrow diameter distributions, nanofibrous scaffolds possess large surface area for cell adhesion and interconnected pore structure, which provides nutrient supply to the cells [12]. There are various methods to fabricate nanofibrous scaffolds for bone regeneration applications; such as self-assembly [13], phase separation [8], template synthesis [14], and electrospinning [15, 16]. Among them, electrospinning is regarded as a simple, economical and versatile method capable of providing continuous ultrafine fibers, which can replicate the nanoscale properties of the natural extracellular matrix (ECM) [17, 18]. It has been proved that the biological features for nanofibrous scaffolds such as hydrophilicity, mechanical strength, biocompatibility, and biodegradability depend on the compositions of the materials utilized for tissue engineering scaffolding [19]. As natural bone is a composite from several components, scaffold for bone tissue engineering, if prepared by means of single material, cannot supply necessary cues for cellular growth. However, if a combination of two or more materials is used to scaffold fabrication, might cause a synergistic effect to create the necessary mechanical strength to the scaffold as well as allow cell attachment, proliferation and differentiation [20, 21]. Nowadays, researchers have been focusing on making scaffolds consisting of multi-polymers and bioactive materials to resemble the characteristics of extracellular matrix (ECM), which also comprises of multi-polymers and biominerals like poly(ε-caprolactone)/gelatin/HA [22], gelatin/chitosan/SiO_2 [23], poly(ε-caprolactone)/fibroin/HA [24], sodium alginate/poly(vinyl alcohol)/zinc oxide [25] and etc. Although there are a variety of natural polymers used in scaffold fabrication, chitosan (CS), a fully or partially deacetylated chitin, has been extensively used as a scaffold material in biomedical field due to its structural similarity with glycosaminoglycan, antibacterial and anticorrosion properties, high biocompatibility, osteoinductive properties, commercial availability at relatively low cost, and non-requirement for any crosslinking agents [26–28]. In spite of the promising potential of chitosan, it has relatively low mechanical strength [29]. For better mechanical properties, it can blend with synthetic polymers such as, poly (ε-caprolactone)-poly(ethylene glycol)-poly(ε-caprolactone) (PCL-PEG-PCL, PCEC) and nanoceramics. PCL-PEG-PCL is a biodegradable, biocompatible, synthetic and non-toxic copolymer of PCL and PEG and has been used as a substrate in a number of biomedical applications [17] because it can develop several blends, composites, and also can integrate with bioactive molecules without changing their biological properties [30, 31]. The use of nanoceramic particles in the fabrication of scaffolds for bone tissue engineering can incorporate nanotopographic features that resemble the structure of natural bone [20]. Silicon dioxide (SiO_2) is necessary in the formation of hard tissues. The first reports of silicon dioxide physiological role have shown that it is involved in the early stage of bone calcification [23, 32]. Silicate bioactive glasses is osteoinductive and bonds with the surrounding tissue because of the interaction of the Si–OH groups with calcium and phosphate ions, resulting in the crystallization of apatite crystals, cell adhesion and collagen formation [32–34]. Silicon is necessary in the formation of hard tissues. The first reports of silicon physiological role have shown that it is involved in the early stage of bone calcification [23, 32]. Silicate bioactive glasses is osteoinductive and bonds with the surrounding tissue because of the interaction of the Si–OH groups with calcium and phosphate ions, resulting in the crystallization of apatite crystals, cell adhesion and collagen formation [32–34]. The excellent biocompatibility and the positive biological properties of silicate bioactive glasses have maintained them in the center of biomaterials research for many decades [35, 36]. Hydroxyapatite (HA) is considered the most widely used inorganic biomaterial for bone replacement therapies since it is similar to the bone mineral phase and has excellent biocompatibility, bioactivity, and osteoconductivity [37–39]. The inclusion of nano-HA (n-HA) has been proven to supply a desired environment for cell response and proliferation by increasing surface roughness and thereby absorption of chemical species from surrounding environment [40]. In the present study, our aim is to fabricate nanofibrous scaffolds of PCEC-CS incorporated with nanoceramics like n-HA and nano-SiO_2 (n-SiO_2) by electrospinning method and to assess the effect of these nanoparticles on physical properties, mechanical properties, and human dental pulp stem cells (hDPSCs) response of the nanofibrous scaffolds. Fourier transform infrared spectroscopy (FT-IR), field

emission scanning electron microscope (FE-SEM), contact angle and mechanical test were applied to evaluate the morphology and chemical properties of nanofibers. Moreover, the effect of nanoparticles on spreading, proliferation and osteogenic differentiation of hDPSCs were assessed.

2 Materials and methods

2.1 Materials

ε-Caprolactone (ε-CL), poly(ethylene glycol) (PEG) with Mw 4000, stannous 2-ethyl hexanoate (stannous octoate, $Sn(Oct)_2$), tetraethylorthosilicate (TEOS) and glutaraldehyde (25%) were purchased from Sigma-Aldrich Co. (Steinem, Germany). Chitosan (degree of deacetylation 85% and Mw = 100,000–300,000) was supplied from Acros chemical Co. Calcium hydroxide [$Ca(OH)_2$], dimethyl sulfoxide (DMSO), n-hexane, ammonium hydroxide (NH_4OH), orthophosphoric acid (H_3PO_4), absolute methanol (MeOH), acetone and formic acid were all obtained from Merck Chemical Co. Phosphate buffer fetal bovine serum (FBS), phosphate buffered saline (PBS) and Dulbecco's modified Eagle medium (DMEM) were procured from Gibco, Singapore. 3-(4,5-Dimethylthiazol-2-yl-2, 5-diphenyltetrazolium bromide) (MTT) was obtained from Invitrogen (Carlsbad, CA, USA).

2.2 Synthesis of PCEC copolymer

Three block copolymers PCEC were prepared by ring opening polymerization of ε-caprolactone in presence of PEG of Mw 4000 and stannous octoate [$Sn(Oct)_2$] [17]. Briefly, a known amount of ε-caprolactone (20.0 g, 175 mmol), PEG (2.0 g, 0.5 mmol) and $Sn(Oct)_2$ (0.5 wt%) was placed in the 50 ml round-bottom flask. The system was heated to 130 °C under nitrogen atmosphere and the polymerization was performed for 12 h. The resulting product was solubilized in methylene chloride followed by precipitation in an excess of cold hexane to remove unreacted species. The molecular weight of PCEC was equal to 45454 g/mol.

2.3 Synthesis of nano-HA particles

The nano-HA particles were obtained in-house by the reaction of calcium hydroxide [$Ca(OH)_2$] with orthophosphoric acid (H_3PO_4):

$$10\ Ca(OH)_2 + 6\ H_3PO_4 \rightarrow Ca_{10}(PO_4)_6(OH)_2 + 18\ H_2O$$

Briefly, 100 mL of 0.3 M H_3PO_4 solution was dropped into 100 mL of 0.5 M $Ca(OH)_2$ solution to produce a white precipitate. The PH of the solution was maintained above 10 by the addition of ammonium hydroxide (NH_4OH) within the sedimentation process. The resulting precipitate remained in the same solution for 5 days. After extensively washed by ultrapure deionized water, the resulting nanoparticles were dried in an oven at 110 °C for 2 h [41, 42].

2.4 Synthesis of nano-SiO_2 particles

Silica nanoparticles were synthesized by sol–gel method as explained previously by our group [43]. Briefly, 1.98 g (10 mmol) H_2O, 60 mL (10 mmol) NH_4OH and 100 mL absolute MeOH were added to a 250 mL round-bottom flask. The solution was kept under stirring for 5 min. Then, 10.41 g (500 mmol) TEOS was dropped into the reaction media. After the final solution was kept for 3 days at room temperature, the resulting nanoparticles were precipitated with n-hexane and collected by centrifugation at 14,000 rpm. Finally, the obtained powders were freeze-dried for 24 h.

2.5 Fabrication of nanofibrous scaffolds by electrospinning

To prepare the 9 wt% PCEC and 2 wt% CS solutions, PCEC and CS were dissolved separately in formic acid/acetone (10:3 v/v) solvent mixture. PCEC and CS solutions were then mixed in a volume ratio of 80:20 and kept stirring for 12 h. For electrospinning of polymeric solutions containing n-HA and n-SiO_2, a known amount of these particles (10 and 15% wt with respect to the total weight of polymers) was mixed with the PCEC-CS solution to provide two different concentration of each nanoparticle. For the preparation of nanofibrous scaffolds by electrospinning, the polymer solutions of (A) PCEC-CS, (B) PCEC-CS/10HA, (C) PCEC-CS/15HA, (D) PCEC-CS/10SiO_2 and (E) PCEC-CS/15SiO_2 were separately placed in a 5 ml plastic syringe which is attached to a blunt-ended needle with tip diameter of 16-gauge. The flow rate of polymeric solutions was adjusted at 0.8–1 mL/h, and the applied voltage of 16–19 kV and a distance of 90–110 mm between the needle tip and collector were optimized through electrospinning process. The nanofibrous samples were produced at room temperature and the humidity at a range of 12–17%. On application of parameters cited nanofibers were spread on metal collector wrapped with an aluminum foil with the dimension of 2 × 20 cm^2.

2.6 Electrospun nanofibrous scaffold characterizations

FT-IR spectra of samples were recorded on a Bruker-Tensor 270 spectrometer in the frequency range between 4000 and 400 cm^{-1}. XRD tests were observed by a Bruker Discover

X-ray diffractometer (Karlsruhe, Germany) diffractometer. The analysis of samples was carried out at 40 kV and 40 mA using the Cu-Kα radiation in 2θ range of 5°–70°. The surface morphology of the electrospun fibers was studied with FE-SEM type 1430 VP (LEO Electron Microscopy, Cambridge, UK). Before SEM imaging, the samples were vacuum-coated with a gold layer using a sputter coater unit (Polaron SC7620) and observed under SEM at 10 kV. n-HA and n-SiO_2 particles size, fiber diameters and their distribution were determined by random selecting of at least 60 different mat segments by using image J software. The specific surface area of n-HA and n-SiO_2 particles was measured by the Brunauer–Emmett–Teller (BET, NOVA 2000 SERIES N20-14, Boynton Beach, FL, USA). The distribution of n-HA and n-SiO_2 within the PCEC-CS nanofibrous scaffolds was evaluated by means of a transmission electron microscope (TEM, Phillips, Eindhoven, Netherlands) at an operating voltage of 100 kV. For TEM observations, the nanofibers were directly electrospun onto copper/carbon grids for 10 s and then dried. Thermogravimetric analysis was performed by TGA (Mettler Toledo, TGA/SDTA 851 e, Columbus, OH, USA) to assess the thermal decomposition of the nanofibrous scaffolds. All the nanofibers were weighed and run at the temperature ranging from 50 to 800 °C at a rate of 10 °C per minute in the nitrogen atmosphere. The tensile strength of nanofibrous composite scaffolds was tested using a Zwick tensile testing machine (Z010, Zwick/Roell, Ulm, Germany). Strip-shape samples of PCEC-CS, PCEC-CS/HA (10 and 15 wt%), and PCEC-CS/SiO_2 (10 and 15 wt%) scaffolds (10 mm × 50 mm × 0.06 mm) were utilized for testing with a 10 N load cell and at an extension rate of 5 mm/min. The mechanical tests were repeated in triplicate for each sample. Tensile stress, strain, and elastic modulus were estimated based on the resulted tensile stress–strain curves [22]. The wettability of the fabricated nanofibrous scaffolds was measured by drop water contact angle instrument (Data Physics Instruments GmbH, Filderstadt, Germany). A drop of deionized water with a size of 5 μL was dropped onto the surface of the scaffolds and images were taken at 5 s to characterize the wetting ability of each scaffold. All of the experiments were done at 25 °C.

2.7 *In vitro* degradation

In order to evaluate the *in vitro* degradation of PCEC-CS nanofibers with different n-HA and n-SiO_2 contents, the nanofibrous scaffolds were weighed (W_0), placed in PBS-medium containing lysozyme (10,000 U/ml), and then incubated at 37 °C for a period of time. At preselected time point, the nanofibrous scaffolds were taken out, washed thoroughly with water, dried at room temperature, and then weighed (W_t). Values are mean ± SD (n = 3). Weight loss (%) of each sample was calculated from the following formula:

$$\text{Weight loss } (\%) = (W_0 - W_t)/W_0 \times 100$$

2.8 Isolation and characterization of hDPSCs

Recently, the procedure of isolation and characterization of human dental pulp stem cells (hDPSCs) was reported by our group [30]. These cells were extracted from primary and permanent teeth and were determined by FACS (Fluorescence-activated cell sorting). The regeneration of bone using hDPSCs cultured on appropriate composite nanofibrous scaffolds was evaluated at this study. All experimental protocols were approved by the Ethics Committee of Tabriz University of Medical Sciences (TUMS) which was in compliance with Helsinki declaration, and all participants signed the informed consent (Approval No. 56/6925) [44].

2.9 Cell proliferation analysis by the MTT test

Before cell culturing, nanofiber mats (10 mm × 10 mm × 0.06 mm) were weighed (10 mg) and transferred to 24-well plates, soaked 3 times in a 70% EtOH solution for 20–30 min. After evaporation of EtOH in the air, nanofibrous mats were washed with PBS and incubated in DMEM for one day. hDPSCs were cultured in DMEM amplified with 10% fetal bovine serum (FBS, Cambrex, East Rutherford, NJ, USA), 100 U mL^{-1} penicillin (Gibco BRL, Grand Island, NY, USA), and 100 μg mL^{-1} streptomycin (Gibco BRL, Grand Island, NY, USA), 1X amphotericin B and were incubated at 37 °C in a 5% CO_2 incubator. When cell density reached 70–80% confluency, they were harvested by 0.05%-trypsin containing 1 mM EDTA solution. Cell population were accounted by hematocytometer and viable cells were numerated by trypan blue analyze. After completely detaching culture medium from scaffolds, stem cells were subcultured on the nanofibrous scaffolds at a density of 20,000–30,000 cell/well and incubated to allow cells distribution and cell attachment throughout the scaffolds. The medium was changed every day. Cell culturing tests were carried out triplicate for each sample. The proliferation of cells was measured by MTT assay. After 3, 7 and 12 days, the medium was refreshed and 500 μL of MTT solution (2 mg/mL in PBS (pH 7.4)) were added to each well and then incubated for 4 h. Next, supernatants were discarded and DMSO was added to wells to dissolve blue furmazan crystals. The absorbance of samples was taken at 570 nm using an ELISA reader. The stem cells cultured on tissue culture plates (TCPs) were considered as control group.

2.10 DAPI staining

DAPI (4,6-diamidino-2-phenylindole) staining was also carried out to examine the cell attachment and proliferation

Table 1 Sequences of primers used for QRT-PCR

Name	Forward	Reverse
BMP2	GAGAAGGAGGAGGCAAAGAAAAG	GAAGCAGCAACGCTAGAAGAC
BGLAP	ATTGTGGCTCACCCTCCATCA	AGGGCTATTTGGGGGTCATC
DSPP	CTGGTGCATGAAGGTGATAGAG	TCCTACTTCTGCCCACTTAGA
RUNX2	ACCTTGACCATAACCGTCTTC	GGCGGTCAGAGAACAAACTA
GAPDH	CAAGATCATCAGCAATGCCTCC	GCCATCACGCCACAGTTTCC

on the nanofibrous scaffolds for 12 days. The cell-seeded constructions were washed with PBS solution, fixed with 4% phosphate-buffered paraformaldehyde at room temperature for 20 min, and then rinsed with PBS. The cells were permeabilized with 0.1% Triton-X100 (Sigma-Aldrich, St. Louis, MO, USA) in PBS for 5 min, washed with PBS, and followed by staining with 0.1 μg/mL of DAPI (Sigma-Aldrich, St. Louis, MO, USA). Subsequently, the samples were rinsed with PBS and visualized with a fluorescent microscope (Olympus IX81, Hamburg, Germany).

2.11 Cell morphology study

Morphological studies of the adhered hDPSCs on the electrospun scaffolds were carried out after 14 days of *In vitro* cell culture, by means of FE-SEM analysis. The electrospun nanofibers were washed twice with PBS and fixed in 2.5% glutaraldehyde. Subsequently, electrospun scaffolds were dehydrated with calibrated concentration of EtOH (50, 75, 90 and 100%) and then air-dried at 25 °C, and their morphology evaluated by FE-SEM.

2.12 Alizarin red S assay

Alizarin red S (ARS) staining was employed to evaluate the calcium mineralization. It was carried out as defined by Stanford et al. [45, 46]. Briefly, the constructs were rinsed three times by PBS and fixed in 70% (v/v) cold ethanol for 1 h. These ethanol-fixed constructions were washed with water and then incubated with 40 mM ARS solution for 20 min. Composite scaffolds with no hDPSCs were applied to remove the background. After washing several times with water, these constructs were destained with 10% (w/v) cetylpyridinium chloride in 10 mM sodium phosphate for 15 min. Afterwards, ARS levels were determined by absorbance measurement at 570 nm.

2.13 QRT-PCR

After 21 days of hDPSCs seeding on electrospun scaffolds, the media was removed and then rinsed with PBS. Total RNA Kit (Bio basic, Toronto, Canada) was utilized to extract the total RNAs from all of the treatment samples and hDPSCs used as control group. The gel electrophoresis and Nanodrop (Thermo Scientific, Waltham, MA, USA) were applied for the determination of extracted RNA yield and value. The total RNA (1 μg) was utilized for cDNA synthesis using a Revertide cDNA synthesis kit (Fermentase, Life Science, USA). To real-time PCR, cDNA was mixed with Syber green Master Mix (Ampliqon, Odense M, Denmark) and specific primers of BGLAP, DSPP, BMP2, Runx2 and GAPDH as housekeeping gene. Primer sequences were offered in Table 1. The PCR data were evaluated using the ΔΔCt method.

2.14 Statistical analysis

The statistical comparisons of different groups were conducted based on ANOVA and *T* test where $p < 0.05$ was regarded as significant. The experiments were carried out in triplicate.

3 Results and discussion

3.1 Morphology and structure of nanoparticles

The morphological and structural characterization of nanoparticles was carried out using a series of techniques, including FT-IR, XRD, and FE-SEM. FT-IR spectra of the synthesized n-HA and n-SiO_2 were shown in Fig. 1A. In the IR spectra of n-HA, the absorption peaks at 451, 574, 601 and 1041 cm^{-1} corresponded to P-O vibrations of phosphate groups (PO_4^{3-}). The broad peak at 3429 cm^{-1} was related to the stretching vibrations of hydroxyl groups (–OH). The peak at 1425 cm^{-1} belonged to the stretching vibration of carbonate group (CO_3^{2-}), which might be entered to n-HA from the atmosphere within synthesis [47]. The observation peaks at 956 and 1083 cm^{-1} in the IR spectra of n-SiO_2 were related to the stretching vibrations of the Si–OH and Si–O–Si groups, respectively. A broad peak at 3402 cm^{-1} was attributed to the stretching vibrations of free-silanol O–H groups. From XRD analysis, the peaks of n-HA were detected at $2\theta = 26.24°$, 31.36°, 39.48°, and 49.64°, the pattern of the synthesized n-SiO_2 showed the presence of the major n-SiO_2 peak at $2\theta = 20.2^{o}$ which was accordance with the standard peak

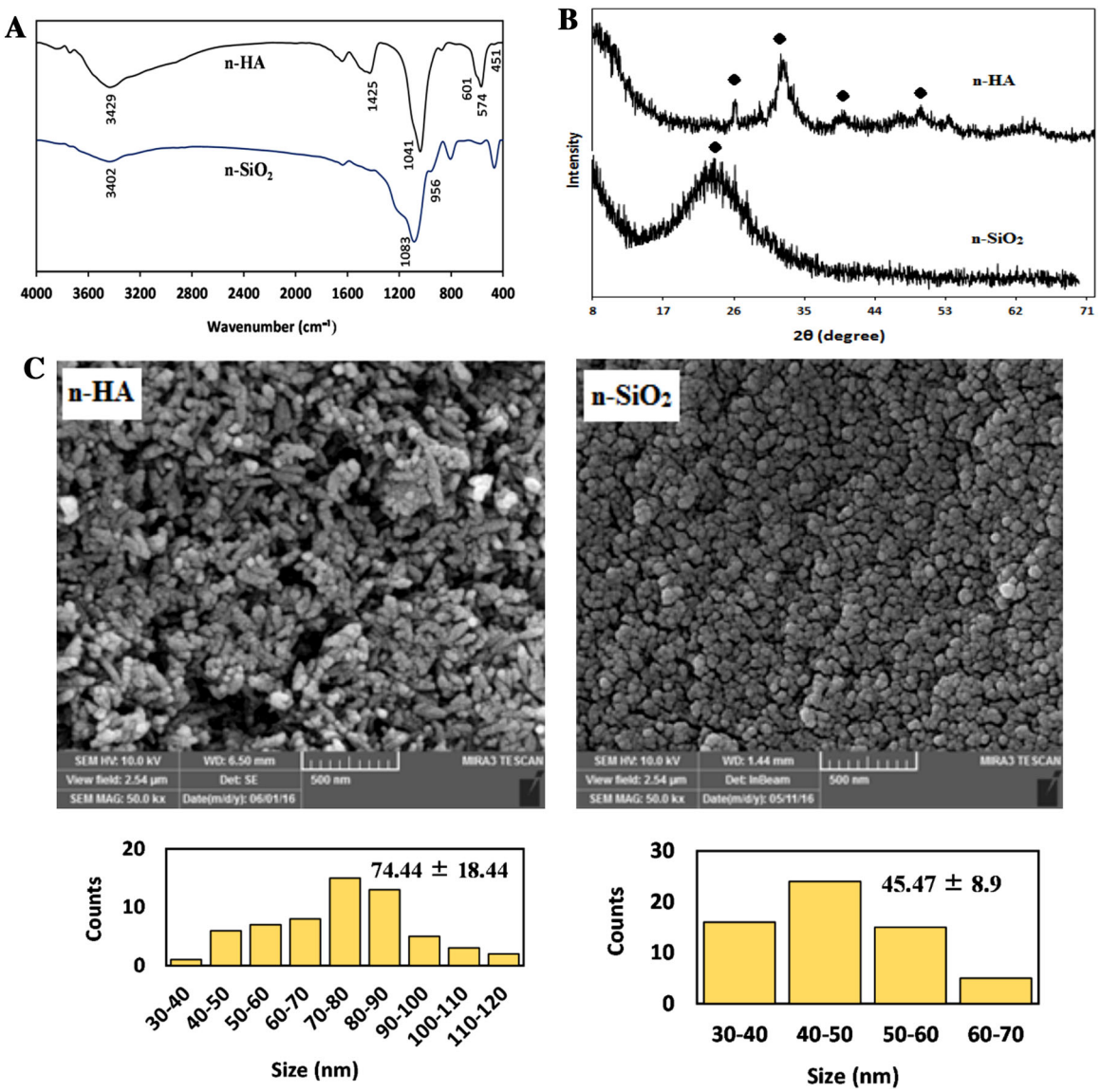

Fig. 1 **A** FT-IR spectra of n-HA and n-SiO_2, **B** XRD patterns of n-HA and n-SiO_2, **C** FE-SEM images of n-HA and n-SiO_2. Scale bars in SEM images = 500 nm

of n-SiO_2 (Fig. 1B) [48]. FE-SEM evaluation of nanoparticles revealed that the n-HA and n-SiO_2 particles were uniform in size and shape. As seen in Fig. 1C, the n-HA crystals showed rod-like morphologies with a mean size of 74.44 ± 18.44 nm, while the n-SiO_2 particles showed spherical morphologies with a mean size of 45.47 ± 8.9 nm. The BET analysis of the HA and SiO_2 nanoparticles gave a specific surface area of 131 and 444 m^2/g, respectively.

3.2 Morphology of electrospun nanofibers

The electrospinning of polymer blends is one the most interesting techniques for providing new and desirable scaffolds for tissue engineering applications. Various solvent systems have been used for electrospinning of polymer blends like 1,1,1,3,3,3-hexafluoro-2-propanol (HFIP), and trifluoroethanol (TEF) [49–52]. Due to the high cost of these solvents and their drastic nature, which leads to faster degradation of the polymers, their use is limited. Here, we used formic acid/acetone as a solvent system for electrospinning of PCEC-CS nanofibers containing n-HA and n-SiO_2 as inorganic nanoparticles. This solvent system is cheap and the high conductivity of formic acid leads to the production of high quality fibers. On the other hand, acetone reduces surface tension and produces beadless nanofibers. Acetone also helps to increase the evaporation of the solvent system. To produce bead-free nanofibers with a relatively similar diameter distribution, the process of optimization was done by varying of

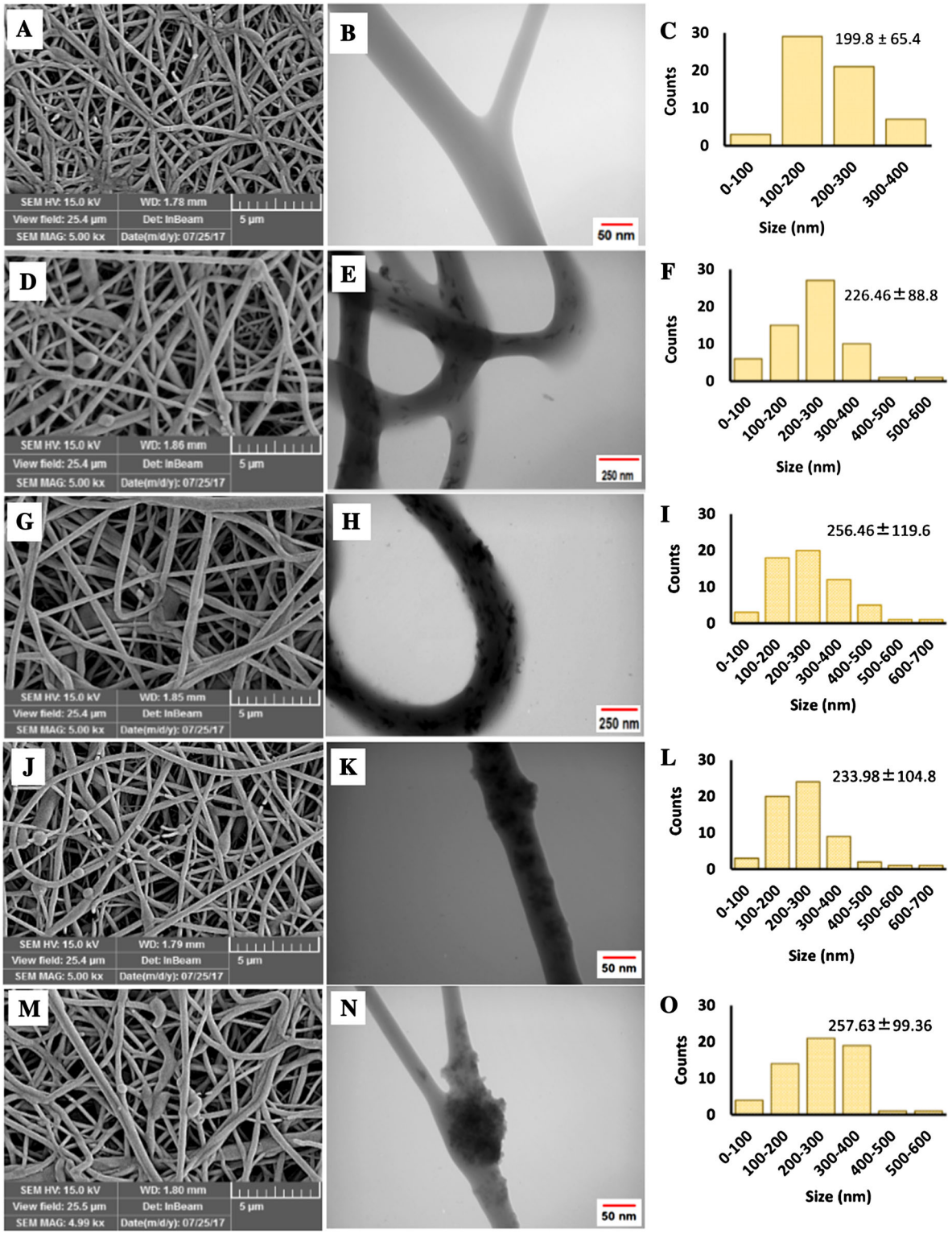

Fig. 2 FE-SEM and TEM images of electrospun scaffolds and the corresponding diameter distributions: **A–C** PCEC-CS, **D–F** PCEC-CS/10HA, **G–I** PCEC-CS/15HA, **J–L** PCEC-CS/10SiO_2, and **M–O** PCEC-CS/15SiO_2. Scale bars in SEM images = 5 µm

different electrospinning parameters. The morphology and diameter distribution of electrospun scaffolds have been demonstrated in Fig. 2. FE-SEM images of nanofibers showed bead-free fibrous structures with smooth surfaces, high porosity and interconnected pores produced under controlled conditions. High porosity and pore

interconnectivity are of the necessities for tissue regeneration as they can offer a suitable 3D microenvironment for cell penetration and also support nutrients and waste exchanges between the scaffold and its environment [53]. TEM images showed the inner structure of nanofibrous scaffolds more obviously. As seen in Fig. 2B, the surface of the PCEC-CS nanofibers was smooth and no nanoparticles were detected. However, the surface of the n-SiO_2 and n-HA incorporated PCEC-CS nanofibers became rough and the distribution of nanoparticles could be observed. As seen in Fig. 2E, K, n-HA and n-SiO_2 particles were well distributed within the fibers with slight agglomeration when the content of nanoparticles was 10 wt%. With the increase of the n-SiO_2 and n-HA contents up to 15 wt%, the agglomeration of the nanoparticles increased and some protrusions were detected on the surface of n-SiO_2 incorporated electrospun scaffolds (Fig. 2H, N). Additionally, with the incorporation of n-SiO_2 and n-HA to PCEC-CS electrospun nanofibers, the fiber diameter increased. The average diameter of PCEC-CS fibers measured from FE-SEM images was 199.8 ± 65.4 nm (Fig. 2C). The samples containing 15% of additives (i.e., PCEC-CS/15HA and PCEC-CS/15SiO_2) had the highest average fiber diameter, 256.46 ± 119.6 nm and 257.63 ± 99.36 nm, respectively (Fig. 2I, O). Whereas the average fiber diameter for samples containing 10% of nanoparticles (i.e., PCEC-CS/10HA and PCEC-CS/10SiO_2) was in the sequence of 226.46 ± 88.8 nm and 233.98 ± 104.8 nm, respectively (Fig. 2F, L). In fact, by introducing nanoparticles into polymeric solutions, the conductivity of the solution decreased, which might affect the spinning behavior of the solution and lead to an increase in the diameter of the mats.

3.3 Characterization of electrospun nanofibers

FT-IR spectroscopy was utilized to analyze the chemical structure of electrospun nanofibers to investigate the presence of scaffold components. As seen in Fig. 3A, the absorption peaks of PCEC were found at 1733 cm^{-1} (ester carbonyl stretching), 1253 cm^{-1} (–COO– stretching) and 1176 cm^{-1} (C–O–C stretching). The characteristic peaks of CS were observed at 1647 cm^{-1} (N–H stretching) and 1095 cm^{-1} (C–O–C bending). These data were consistent with theoretical data [17, 47] and showed that both PCEC and CS were present in the composite scaffold. The chemical structures of PCEC-CS scaffolds containing 10 and 15 wt% n-HA showed the absorption peaks at 451, 576 and 1041 cm^{-1} that were due to P–O vibrations of phosphate groups (PO_4^{-3}) of n-HA. The presence of PCEC was verified by the peaks at 1733, 1253 and 1176 cm^{-1} related to carbonyl stretching, –COO– stretching and C–O–C stretching. The absorption peaks of CS were also observed at 1647 and 1095 cm^{-1} related to N–H stretching and C–O–C bending. The chemical structures of PCEC-CS scaffolds containing 10 and 15 wt% n-SiO_2 showed absorbance peak at 956 cm^{-1} which was related to the stretching vibrations of the Si–OH groups. Similarly, the absorption peaks associated with PCEC and CS were observed in FT-IR spectra of PCEC-CS/SiO_2 (10 and 15 wt%).

TGA thermograms have been used to evaluate the thermal stability and decomposition of nanofibrous scaffolds. Figure 3B showed the TGA diagrams of PCEC-CS, PCEC-CS/10HA, PCEC-CS/15HA, PCEC-CS/10SiO_2, and PCEC-CS/15SiO_2 nanofibers. The maximum thermal degradation temperature of PCEC-CS, PCEC-CS/10HA, PCEC-CS/15HA, PCEC-CS/10SiO_2, and PCEC-CS/15SiO_2 nanofibers was 347, 387, 380, 360, 383 °C, respectively, exhibiting that the incorporation of n-HA or n-SiO_2 nanoparticles improved the heat resistance of PCEC-CS nanofibers. These results are attributed to the excellent insulation and mass-transport barrier features of the inorganic nanoparticles, which slow down the decomposition of the polymeric scaffold [54]. Additionally, the final remaining weight increased with increasing nanoparticle contents.

3.4 Mechanical behaviors of nanofibrous scaffolds

The mechanical characteristics of scaffolds are one of the important factors that need attention in tissue engineering. Since they can affect the cell activities, for example, cell adhesion, proliferation, and differentiation [55, 56]. The effect of n-SiO_2 and n-HA contents on the mechanical properties of PCEC-CS nanofibrous scaffolds were analyzed. As shown in Fig. 4 and Table 2, the mechanical properties of PCEC-CS nanofibrous scaffolds in term of tensile strength and Young's modulus significantly increased by increasing of nanoceramics while the elongation at break reduced. There was also an increase in the mechanical properties of PCEC-CS/10HA and PCEC-CS/15HA compared to its n-SiO_2 incorporated counterparts. High mechanical properties of polymer composites containing nanoceramics are due to the fact that these particles have stiffer mechanical properties than polymers and thus their distribution within polymer matrix provide adequate strength and stiffness that will withstand a certain level of physiological loading so that the scaffolds can function before the new tissue replaces the scaffold matrix which is gradually degrading [57].

3.5 Contact angle of electrospun nanofibers

The surface hydrophilicity is an important index for biomaterials as *in vivo* tissue engineering scaffolds. It can lead to good spreading, attachment and proliferation of cells [58]. The contact angles of the nanofibrous scaffolds were

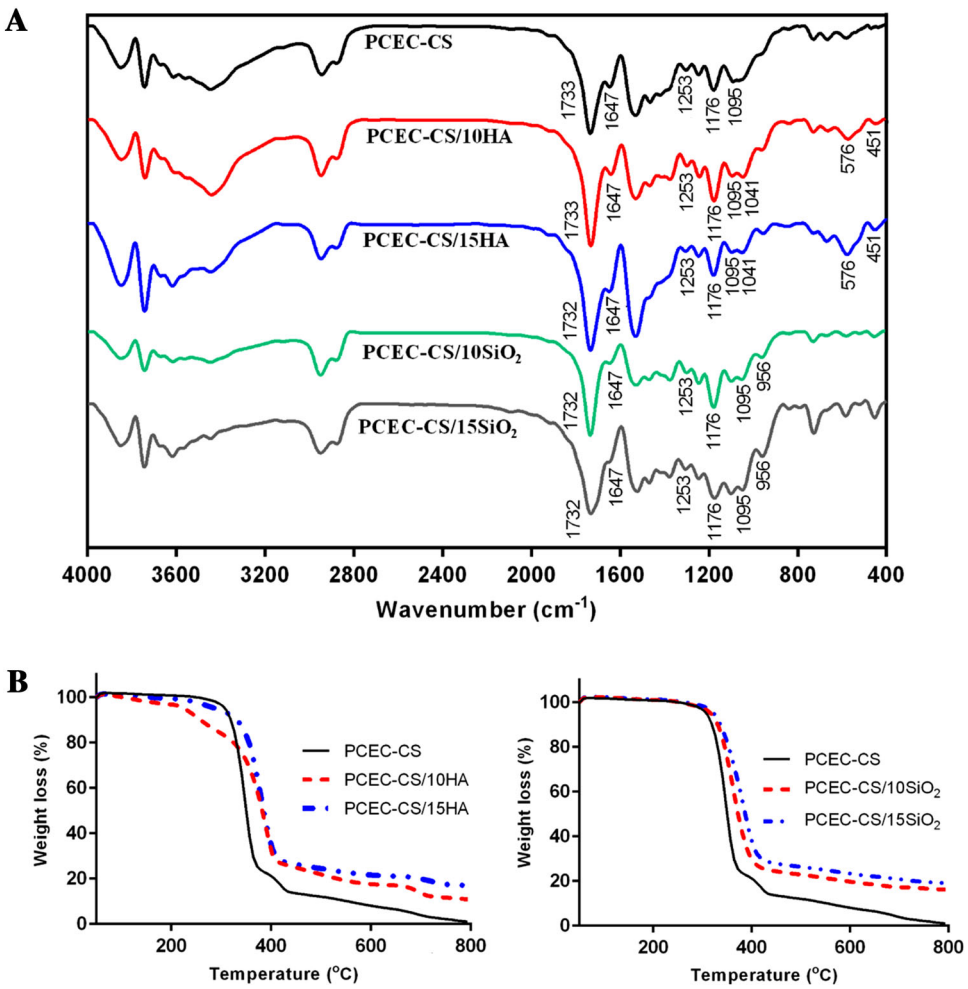

Fig. 3 **A** FT-IR spectra and **B** TGA diagrams of electrospun scaffolds

measured to evaluate the surface hydrophilicity of the scaffolds. The contact angle of PCEC-CS electrospun nanofiber was calculated to be 126.17° ± 0.81°, whereas the scaffolds enriched with nanoparticles had a lesser contact angle, namely, 123.56° ± 2.29°, 101.36° ± 1.84°, 93.07° ± 1.63°, and 70.05° ± 2.36° for PCEC-CS/10HA, PCEC-CS/15HA, PCEC-CS/10SiO_2, and PCEC-CS/15SiO_2, respectively. With the increasing of n-HA and n-SiO_2 contents, the contact angle of scaffolds decreased significantly. The results showed that n-SiO_2 and n-HA nanoparticles improved the surface hydrophilic features due to their high specific surface area. Our observations were in good agreement with previous studies in which the hydrophilicity of scaffolds increased by increasing nanoparticle contents [59, 60]. Photographs of water drops on nanofibrous scaffolds were shown in Fig. 5.

3.6 *In vitro* degradation studies

The biodegradation of the scaffolds is an essential factor in tissue engineering. In an ideal scenario, the scaffolds must

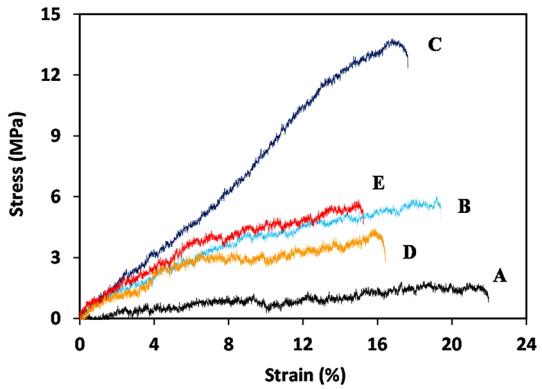

Fig. 4 The stress–strain curves of electrospun scaffolds: **A** PCEC-CS, **B** PCEC-CS/10HA, **C** PCEC-CS/15HA, **D** PCEC-CS/10SiO_2, and **E** PCEC-CS/15SiO_2

be degraded at a rate that the formation of new tissue takes place [57]. Figure 6 exhibited weight loss of PCEC-CS, PCEC-CS/10HA, PCEC-CS/15HA, PCEC-CS/10SiO_2, and PCEC-CS/15SiO_2 nanofibers against incubation time in PBS solution (PH = 7.4) at 37 °C. It could be seen that with the increase of degradation time, the weight loss of all

Table 2 Mechanical properties of PCEC-CS nanofibers with different n-HA and n-SiO_2 contents

Sample	Tensile strength (MPa)	Elongation at break (%)	Young's modulus (MPa)
PCEC-CS	2.75 ± 0.56	23.5 ± 0.98	57.35 ± 1.2
PCEC-CS/10SiO_2	4.84 ± 0.25	16.3 ± 0.63	61.97 ± 0.36
PCEC-CS/15SiO_2	6.01 ± 0.87	15.68 ± 1.25	88.44 ± 0.25
PCEC-CS/10HA	6.55 ± 1.12	19.38 ± 5.2	194 ± 0.89
PCEC-CS/15HA	14.33 ± 0.36	17.88 ± 2.36	183 ± 6.5

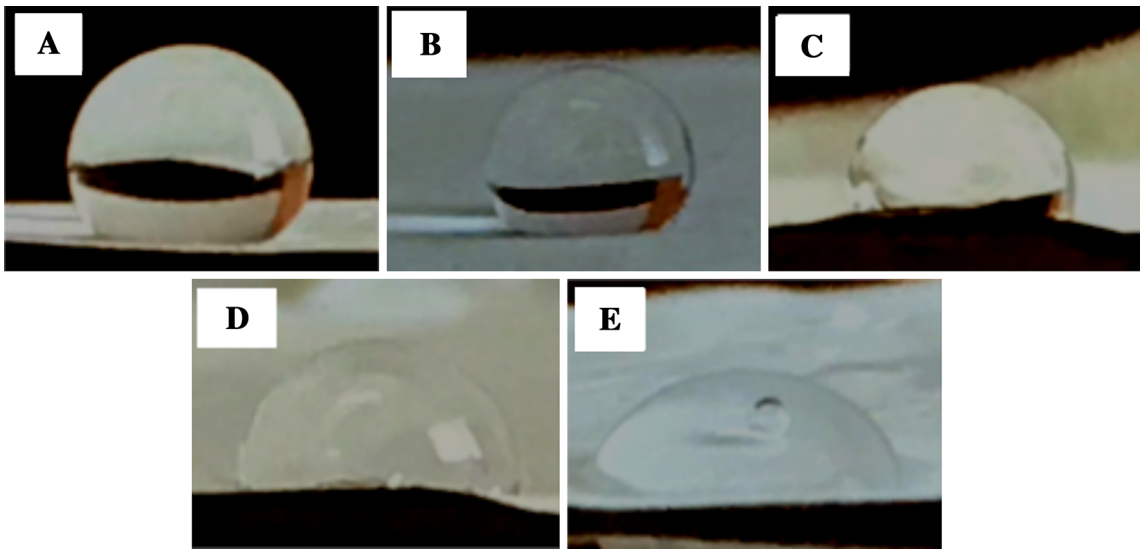

Fig. 5 Water contact angles of electrospun scaffolds: **A** PCEC-CS, **B** PCEC-CS/10HA, **C** PCEC-CS/15HA, **D** PCEC-CS/10SiO_2, and **E** PCEC-CS/15SiO_2

nanofibrous scaffolds improved, although the weight loss was minor in all samples. After 6 weeks *in vitro* degradation, the percentage of weight loss was almost 7.76% in the case of PCEC-CS without nanoparticles, whereas it was higher in the case of n-SiO_2 and n-HA incorporated PCEC-CS nanofibrous scaffolds over the same period. PCEC-CS/10HA, PCEC-CS/15HA, PCEC-CS/10SiO_2, and PCEC-CS/15SiO_2 nanofibers lost 9.22, 10.16, 11.25, and 12.26% weight at the end of the *in vitro* degradation studies, respectively. According to results, the degradation rate of nanofibers improved with the increase of nanoparticles content. These results might be due to high hydrophilicity of nanocomposite nanofibrous scaffolds compared to PCEC-CS nanofibers.

3.7 MTT assay

In order to evaluate the proliferation rate and viability of hDPSCs in nanofibrous scaffolds, an MTT assay was performed. Figure 7A presented the cell viability values of hDPSCs cultured on the TCPS containing DMEM without nanofibers as control, PCEC-CS, PCEC-CS/10HA, PCEC-CS/15HA, PCEC-CS/10SiO_2, and PCEC-CS/15SiO_2

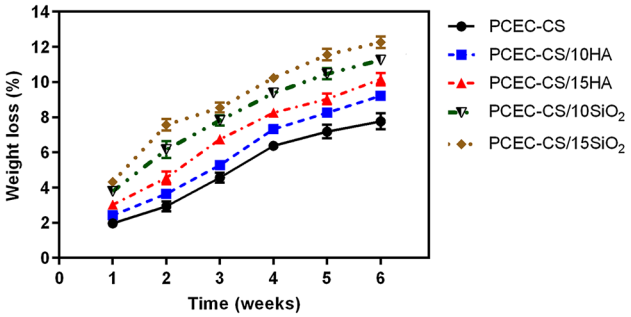

Fig. 6 *In vitro* degradation of electrospun scaffolds after 6 weeks

nanofibrous scaffolds after 3, 7 and 12 days. As seen in Fig. 7A, the cell viability increased by increasing exposure time. In comparison to the behavior of TCP-grown cells with DMEM, the PCEC-CS scaffolds could be introduced to be non-toxic, and therefore biocompatible for hDPSCs. The viability of hDPSCs was almost same in all fiber types on the third day, and n-SiO_2 and n-HA contents had no noticeable effect on OD values. However, at 7th and 12th days, the cell viability increased on all types of fibers, especially in the scaffolds containing nanoparticles. This increase was particularly significant on the 12th day. Based on MTT assay results on day 12, the scaffolds enriched

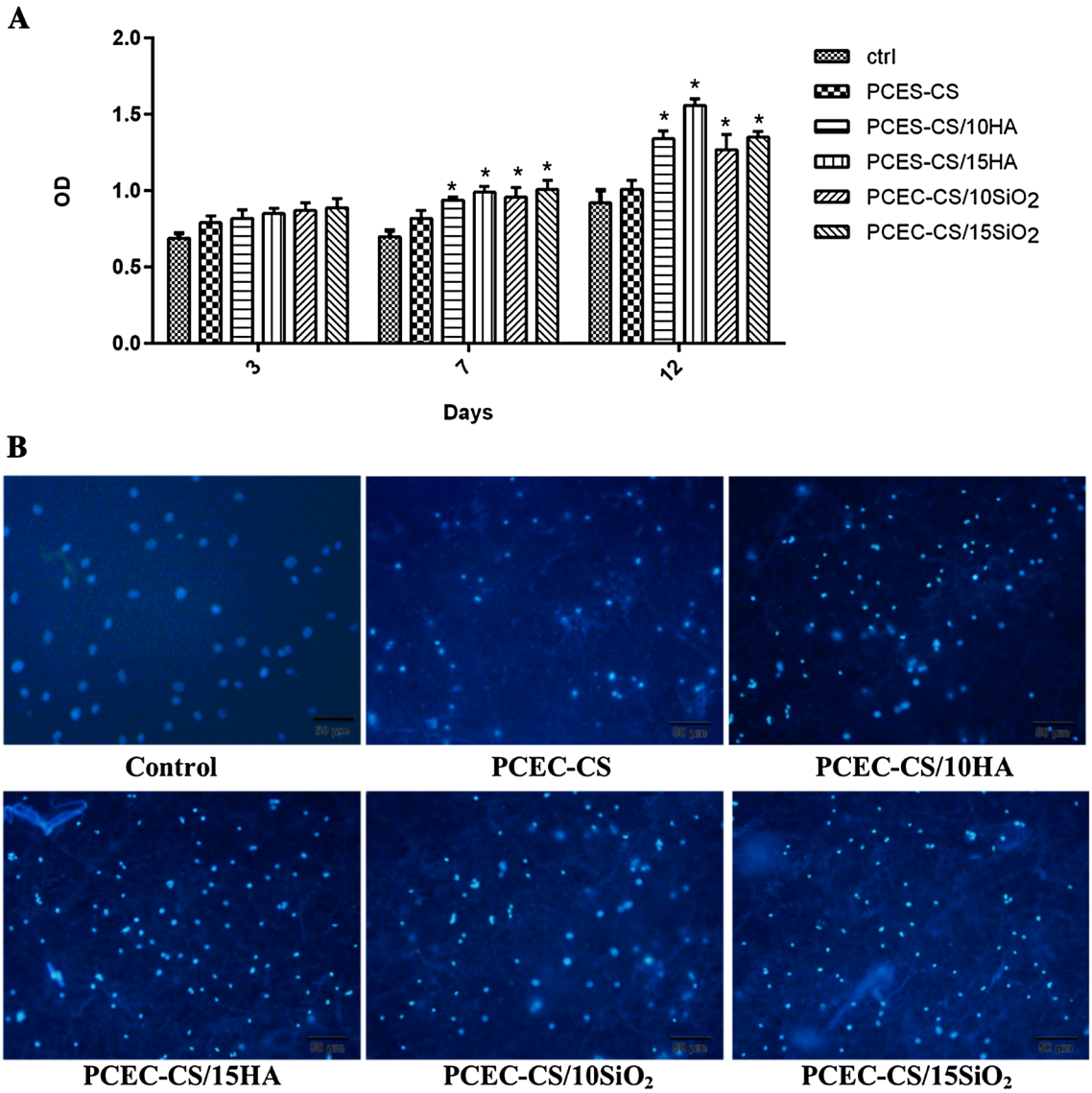

Fig. 7 **A** MTT assays for cell viability study of hDPSCs combined with PCEC-CS nanofibrous scaffolds with different n-HA and n-SiO_2 contents cultured for 3, 7, and 12 days. The n-HA and n-SiO_2 contents were biocompatible for hDPSCs and higher cell numbers were observed in treatment groups. *$p < 0.05$. **B** DAPI staining of hDPSCs cultured on electrospun scaffolds after 12 days of culture

with different ratios of n-HA showed higher hDPSCs proliferation rates as compared to ones enriched with n-SiO_2. PCEC-CS/15HA had the highest cell proliferation rate. Indeed, the introduction of nanoparticles into the structure of scaffolds improved cell anchoring and accelerated hDPSCs proliferation. The reason for which could be related to the excellent bioactivity of nanoparticles that ultimately led to better hydrophilicity and good adhesion and proliferation. Therefore, the presence of n-SiO_2 and n-HA nanoparticles in the nanofiber structure was advantageous for accelerating cell proliferation.

DAPI staining of hDPSCs proliferated on the TCPS containing DMEM without nanofibers as control, PCEC-CS, PCEC-CS/10HA, PCEC-CS/15HA, PCEC-CS/10SiO_2, and PCEC-CS/15SiO_2 scaffolds was shown in Fig. 7B. Cell imaging demonstrated that hDPSCs were well distributed and attached on all types of groups. More hDPSCs were attached on PCEC-CS nanofibers incorporated with n-HA and n-SiO_2 in comparison to bare PCEC-CS nanofibers. PCEC-CS/HA nanofibrous scaffolds exhibited a slight difference in DAPI staining compared to PCEC-CS/SiO_2 nanofibers. It seems that PCEC-CS incorporated with n-HA shewed higher cell adhesion compared to other samples.

3.8 hDPSCs adhesion and proliferation studies on electrospun scaffolds

Figure 8 showed the FESEM images of the morphology of hDPSCs attached on the PCEC-CS, PCEC-CS/10HA,

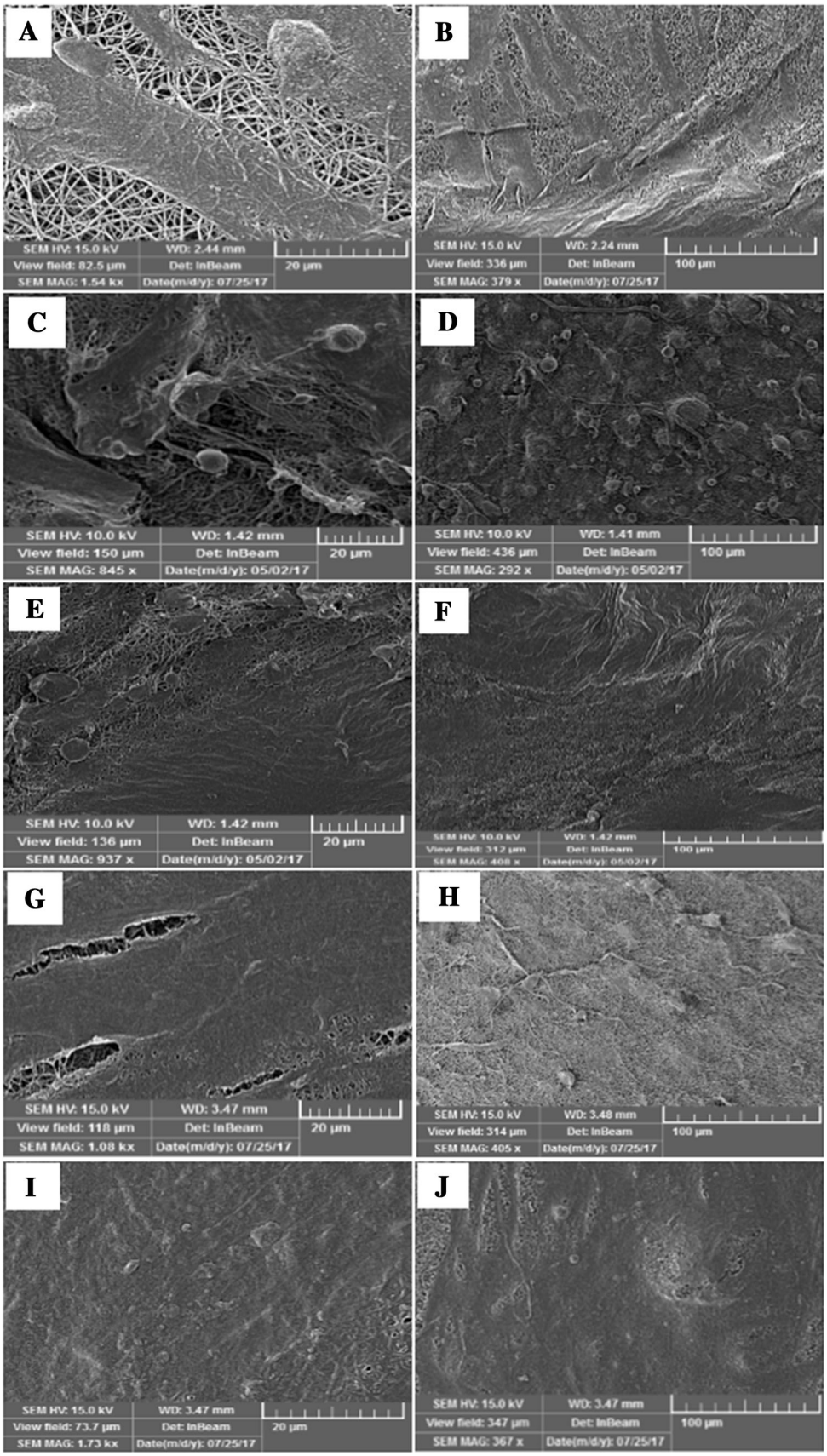

Fig. 8 FE-SEM images of hDPSCs adhesion and spreading on electrospun scaffolds after 14 days of culture: **A, B** PCEC-CS, **C, D** PCEC-CS/10HA, **E, F** PCEC-CS/15HA, **G, H** PCEC-CS/10SiO_2, and **I, J** PCEC-CS/15SiO_2. Scale bars: (**A**, **C**, **E**, **G**, and **I**) = 20 µm, (B**, D**, **F**, **H**, and **J**) = 100 µm

PCEC-CS/15HA, PCEC-CS/10SiO_2 and PCEC-CS/15SiO_2 nanofibrous scaffolds after 14 days of culture. Cell adhesion and proliferation studies with hDPSCs after 14 days revealed more favorable cell attachment morphology in all nanofibrous scaffolds. As seen in the FESEM micrographs, hDPSCs cultured on the control PCEC-CS scaffold could attach and scattered adequately on the surface of the scaffold. They showed a cortical cell morphology. The flat spread out of hDPSCs on the nanofibrous scaffolds indicated a very intense cell attachment and proved a good cytocompatibility and close interaction of scaffolds with cells. The interconnected pores in the nanofibers were covered by hDPSCs and created long cell processes. The evaluation of cell morphology of hDPSCs seeded on nanofibers containing n-HA and n-SiO_2 showed that hDPSCs were able to attach and fully dispersed in the whole area of nanofibers and produced continuous cell sheets on them so that the underlying scaffolds would not be visible. The reason was that nanoceramics could create a better space for the cells due to the high surface area of incorporated nanoparticles and cause more favorable integration of cells with scaffolds. FE-SEM images may be evidence of the ability of improved scaffolds for adhesion, proliferation, and differentiation of hDPSCs and confirmed the outstanding prospects of these scaffolds toward bone tissue engineering applications.

3.9 Mineralization of hDPSCs

The process by which calcium phosphate is deposited on the surface of the substrate is called mineralization where anionic matrix molecules take up calcium, continued by phosphate ions, and act as nucleation and growth sites resulting in calcification. ARS can form a complex with Ca^{2+} in mineralized ECM and thereby display bright orange-red stains [61, 62]. In order to analyze the effect of n-HA and n-SiO_2 nanoparticles on osteogenic differentiation of hDPSCs, ARS tests were carried out on PCEC-CS nanofibrous scaffolds. Figure 9 shows the ARS activity of hDPSCs cultured on PCEC-CS, PCEC-CS/10HA, PCEC-CS/15HA, PCEC-CS/10SiO_2, PCEC-CS/15SiO_2, and regular growth media (DMEM) used as a control. Compared to regular growth media (DMEM) and PCEC-CS scaffold, hDPSCs cultured in nanofibrous scaffolds containing n-SiO_2 and n-HA nanoparticles exhibited significantly higher degree of ARS activity, mainly related to the formation of an osteo-like phenotype. ARS activity was most noticeable in PCEC-CS/15HA, where the OD values had increased approximately 3.3-fold compared with the control group. Our results highlighted that the addition of n-HA and n-SiO_2 in PCEC-CS scaffolds had a positive effect in simulating of minerals, making them worthy for bone tissue engineering purposes.

3.10 QRT-PCR analysis

This study showed that the blending of n-HA and n-SiO_2 can improve the expression of osteogenic marker genes over control PCEC-CS. The up-regulation of osteogenesis markers in cells seeded at nanofibers is an indicator of better-quality osteogenesis. Therefore, we studied the expression of osteogenic markers in hDPSCs cultured on PCEC-CS scaffolds containing n-SiO_2 or n-HA. As seen in Fig. 10A, BGLAP which encodes for osteocalcin in human [63], showed the highest expression levels in PCEC-CS/

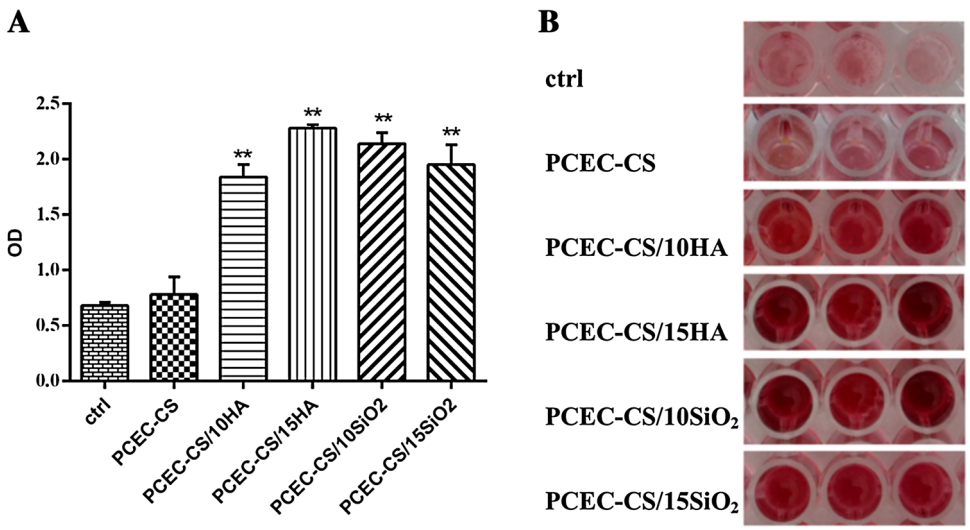

Fig. 9 **A** Alizarin red S staining of hDPSCs osteogenic differentiation cultured on electrospun scaffolds after 16 days of culture. The n-HA and n-SiO_2 incorporated PCEC-CS scaffolds considerably improved osteogenesis potential scaffolds. $^{**}p < 0.01$. **B** hDPSCs were stained with ARS at 16th day to visualize the mineralized bone matrix

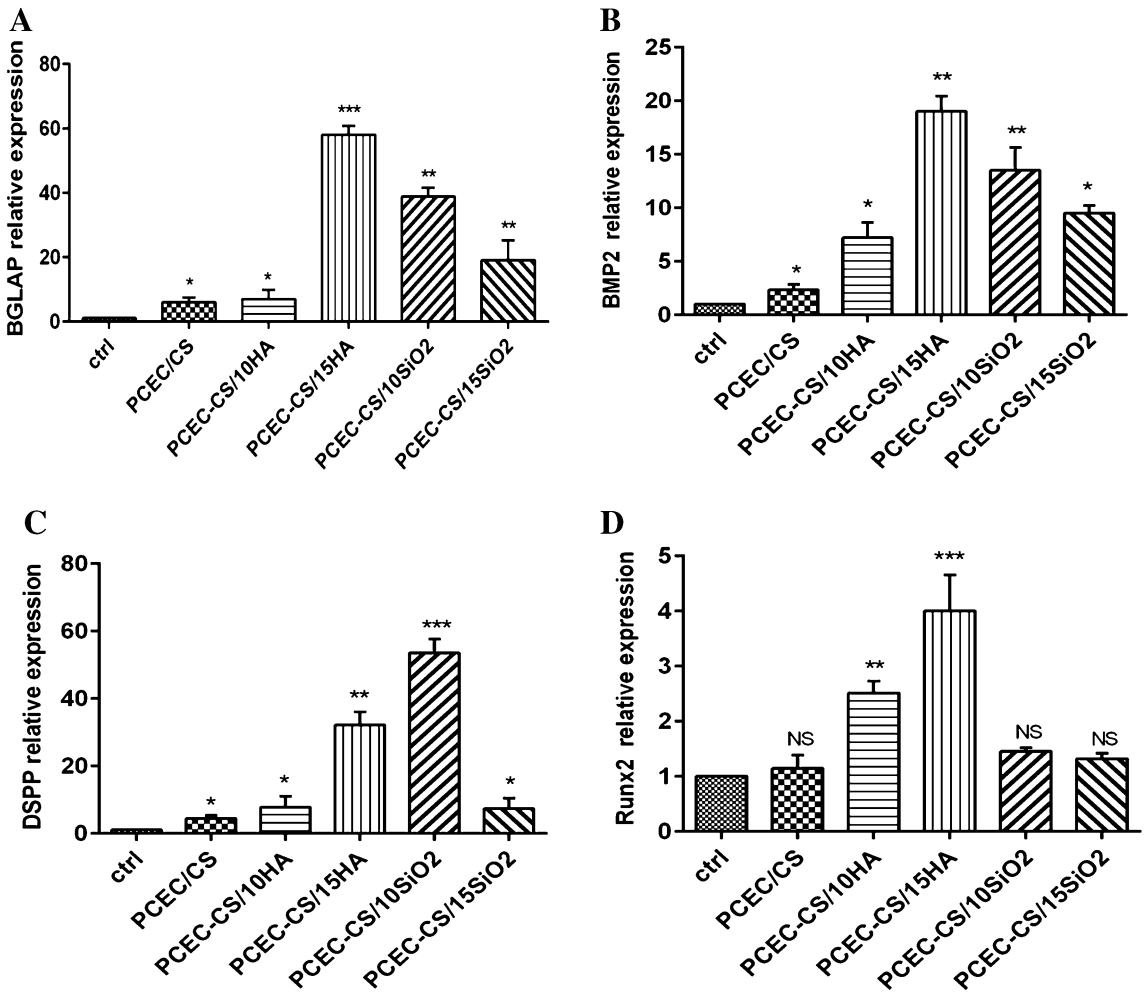

Fig. 10 The QRT-PCR results for expression index of osteogenic marker genes, **A** BGLAP, **B** BMP2, **C** DSPP, and **D** Runx2 in hDPSCs seeded on PCEC-CS, PCEC-CS/10HA, PCEC-CS/15HA, PCEC-CS/10SiO_2, PCEC-CS/15SiO_2 scaffolds and control (without scaffold). *$p < 0.05$, **$p < 0.01$, and ***$p < 0.001$

15HA ($p < 0.001$) and PCEC-CS/10SiO_2 ($p < 0.01$) which demonstrates high osteoconductivity of our treatments. The expression of BMP2 gene in the PCEC-CS/15HA ($p < 0.001$) and PCEC-CS/10SiO_2 ($p < 0.01$) groups was significantly higher than that in the other groups (Fig. 10B). The BMP2 is an important gene in osteogenic induction [64]. Moreover, the expression of DSPP exhibited significant upregulation in PCEC-CS/15HA ($p < 0.01$) and PCEC-CS/10SiO_2 ($p < 0.001$) (Fig. 10C). The DSSP is a key gene in odontogenesis [65]. Additionally, the expression levels of Runx2, as a key transcription factor associated with osteogenic differentiation [66], was higher in n-HA blended scaffolds, however, upon the n-SiO_2 did not show significant upregulation (Fig. 10D). In general, most of the osteogenesis genes become upregulated through n-HA or n-SiO_2 blending of scaffolds. The findings of the present study are in agreement with previous studies of our group which showed positive effects of n-HA on scaffold mediated osteogenic differentiation of DPSCs [66, 67]. Moreover, the present study confirmed the encouraging effect of n-SiO_2 in osteogenic bioengineering.

Acknowledgements The authors were financially supported by a grant (NO: 94/104) from Drug Applied Research Center, Tabriz University of Medical Sciences, Tabriz, Iran.

Compliance with ethical standards

Conflict of interest The authors declare that they have no conflict of interest.

Ethical statement All experimental protocols were approved by the Ethics Committee of Tabriz University of Medical Sciences (TUMS) which was in compliance with Helsinki declaration, and all participants signed the informed consent (Approval No. 56/6925). There are no animal experiments carried out for this article.

References

1. Cancedda R, Dozin B, Giannoni P, Quarto R. Tissue engineering and cell therapy of cartilage and bone. Matrix Biol. 2003;22:81–91.
2. Ghorbani F, Nojehdehian H, Zamanian A. Physicochemical and mechanical properties of freeze cast hydroxyapatite-gelatin scaffolds with dexamethasone loaded PLGA microspheres for hard tissue engineering applications. Mater Sci Eng C Mater Biol Appl. 2016;69:208–20.
3. Bose S, Roy M, Bandyopadhyay A. Recent advances in bone tissue engineering scaffolds. Trends Biotechnol. 2012;30:546–54.
4. Hosseini Y, Emadi R, Kharaziha M, Doostmohammadi A. Reinforcement of electrospun poly (ε-caprolactone) scaffold using diopside nanopowder to promote biological and physical properties. J Appl Polym Sci. 2017;134:44433.
5. Aiyelabegan HT, Zaidi SS, Fanuel S, Eatemadi A, Ebadi MT, Sadroddiny E. Albumin-based biomaterial for lung tissue engineering applications. Int J Polym Mater Polym Biomater. 2016;65:853–61.
6. Lim DJ, Sim M, Heo Y, Jun HW, Park H. Facile method for fabricating uniformly patterned and porous nanofibrous scaffolds for tissue engineering. Macromol Res. 2015;23:1152–8.
7. Koupaei N, Karkhaneh A. Porous crosslinked polycaprolactone hydroxyapatite networks for bone tissue engineering. Tissue Eng Regen Med. 2016;13:251–60.
8. Ma PX, Zhang R. Synthetic nano-scale fibrous extracellular matrix. J Biomed Mater Res. 1999;46:60–72.
9. Gautam S, Dinda AK, Mishra NC. Fabrication and characterization of PCL/gelatin composite nanofibrous scaffold for tissue engineering applications by electrospinning method. Mater Sci Eng C Mater Biol Appl. 2013;33:1228–35.
10. Zhang W, Chen Z, Ma S, Wang Y, Zhang F, Wang K, et al. Cistanche polysaccharide (CDPS)/polylactic acid (PLA) scaffolds based coaxial electrospinning for vascular tissue engineering. Int J Polym Mater Polym Biomater. 2016;65:38–46.
11. Singh RK, Jin GZ, Mahapatra C, Patel KD, Chrzanowski W, Kim HW. Mesoporous silica-layered biopolymer hybrid nanofibrous scaffold: a novel nanobiomatrix platform for therapeutics delivery and bone regeneration. ACS Appl Mater Interfaces. 2015;7:8088–98.
12. Shalumon K, Sowmya S, Sathish D, Chennazhi KP, Nair SV, Jayakumar R. Effect of incorporation of nanoscale bioactive glass and hydroxyapatite in PCL/chitosan nanofibers for bone and periodontal tissue engineering. J Biomed Nanotechnol. 2013;9:430–40.
13. Hartgerink JD, Beniash E, Stupp SI. Self-assembly and mineralization of peptide-amphiphile nanofibers. Science. 2001;294:1684–8.
14. Feng L, Li S, Li H, Zhai J, Song Y, Jiang L, et al. Super-hydrophobic surface of aligned polyacrylonitrile nanofibers. Angew Chem Int Ed Engl. 2002;41:1221–3.
15. Shalumon KT, Binulal NS, Selvamurugan N, Nair SV, Menon D, Furuike T, et al. Electrospinning of carboxymethyl chitin/poly (vinyl alcohol) nanofibrous scaffolds for tissue engineering applications. Carbohydr Polym. 2009;77:863–9.
16. Jie Y, Cai Z, Li S, Xie Z, Ma M, Huang X. Hydroxyapatite nucleation and growth on collagen electrospun fibers controlled with different mineralization conditions and phosvitin. Macromol Res. 2017;25:905–12.
17. Valizadeh A, Bakhtiary M, Akbarzadeh A, Salehi R, Frakhani SM, Ebrahimi O, et al. Preparation and characterization of novel electrospun poly(ε-caprolactone)-based nanofibrous scaffolds. Artif Cells Nanomed Biotechnol. 2016;44:504–9.
18. Bui HT, Chung OH, Cruz JD, Park JS. Fabrication and characterization of electrospun curcumin-loaded polycaprolactone-polyethylene glycol nanofibers for enhanced wound healing. Macromol Res. 2014;22:1288–96.
19. Kouhi M, Morshed M, Varshosaz J, Fathi MH. Poly (ε-caprolactone) incorporated bioactive glass nanoparticles and simvastatin nanocomposite nanofibers: preparation, characterization and in vitro drug release for bone regeneration applications. Chem Eng J. 2013;228:1057–65.
20. Sharma C, Dinda AK, Potdar PD, Chou CF, Mishra NC. Fabrication and characterization of novel nano-biocomposite scaffold of chitosan–gelatin–alginate–hydroxyapatite for bone tissue engineering. Mater Sci Eng C Mater Biol Appl. 2016;64:416–27.
21. Soltani S, Ebrahimian-Hosseinabadi M, Kharazi AZ. Chitosan/graphene and poly (D, L-lactic-co-glycolic acid)/graphene nano-composites for nerve tissue engineering. Tissue Eng Regen Med. 2016;13:684–90.
22. Venugopal JR, Low S, Choon AT, Kumar AB, Ramakrishna S. Nanobioengineered electrospun composite nanofibers and osteoblasts for bone regeneration. Artif Organs. 2008;32:388–97.
23. Kavya KC, Jayakumar R, Nair S, Chennazhi KP. Fabrication and characterization of chitosan/gelatin/SiO_2 composite scaffold for bone tissue engineering. Int J Biol Macromol. 2013;59:255–63.
24. Diaz-Gomez L, García-González CA, Wang J, Yang F, Aznar-Cervantes S, Cenis JL, et al. Biodegradable PCL/fibroin/hydroxyapatite porous scaffolds prepared by supercritical foaming for bone regeneration. Int J Pharm. 2017;527:115–25.
25. Shalumon K, Anulekha K, Nair SV, Nair S, Chennazhi K, Jayakumar R. Sodium alginate/poly(vinyl alcohol)/nano ZnO composite nanofibers for antibacterial wound dressings. Int J Biol Macromol. 2011;49:247–54.
26. Bhattarai N, Edmondson D, Veiseh O, Matsen FA, Zhang M. Electrospun chitosan-based nanofibers and their cellular compatibility. Biomaterials. 2005;26:6176–84.
27. Acevedo CA, Sánchez E, Díaz-Calderón P, Blaker JJ, Enrione J, Quero F. Synergistic effects of crosslinking and chitosan molecular weight on the microstructure, molecular mobility, thermal and sorption properties of porous chitosan/gelatin/hyaluronic acid scaffolds. J Appl Polym Sci. 2017;134:44772–82.
28. Shimojo AAM, Galdames SEM, Perez AGM, Ito TH, Luzo ÂCM, Santana MHA. In vitro performance of injectable chitosan-tripolyphosphate scaffolds combined with platelet-rich plasma. Tissue Eng Reg Med. 2016;13:21–30.
29. Li Z, Ramay HR, Hauch KD, Xiao D, Zhang M. Chitosan–alginate hybrid scaffolds for bone tissue engineering. Biomaterials. 2005;26:3919–28.
30. Zijah V, Salehi R, Aghazadeh M, Samiei M, Alizadeh E, Davaran S. Towards optimization of odonto/osteogenic bioengineering: in vitro comparison of simvastatin, sodium fluoride, melanocyte-stimulating hormone. In Vitro Cell Dev Biol Anim. 2017;53:502-12.
31. Jiang W, Li L, Zhang D, Huang S, Jing Z, Wu Y, et al. Incorporation of aligned PCL–PEG nanofibers into porous chitosan scaffolds improved the orientation of collagen fibers in regenerated periodontium. Acta Biomater. 2015;25:240–52.
32. Kavya KC, Dixit R, Jayakumar R, Nair SV, Chennazhi KP. Synthesis and characterization of chitosan/chondroitin sulfate/nano-SiO_2 composite scaffold for bone tissue engineering. J Biomed Nanotechnol. 2012;8:149–60.
33. Stodolak-Zych E, Frączek-Szczypta A, Wiecheć A, Błazewicz M. Nanocomposite polymer scaffolds for bone tissue regeneration. Acta Phys Pol A, 2012;121:518–21.
34. Lee H, Hwang H, Kim Y, Jeon H, Kim G. Physical and bioactive properties of multi-layered PCL/silica composite scaffolds for bone tissue regeneration. Chem Eng J. 2014;250:399–408.

35. Xynos ID, Hukkanen MV, Batten JJ, Buttery LD, Hench LL, Polak JM. Bioglass® 45S5 stimulates osteoblast turnover and enhances bone formation in vitro: implications and applications for bone tissue engineering. Calcif Tissue Int. 2000;67:321–9.
36. Xynos ID, Edgar AJ, Buttery LD, Hench LL, Polak JM. Ionic products of bioactive glass dissolution increase proliferation of human osteoblasts and induce insulin-like growth factor II mRNA expression and protein synthesis. Biochem Biophys Res Commun. 2000;276:461–5.
37. Jain KG, Mohanty S, Ray AR, Malhotra R, Airan B. Culture & differentiation of mesenchymal stem cell into osteoblast on degradable biomedical composite scaffold: in vitro study. Indian J Med Res. 2015;142:747–58.
38. Venugopal J, Prabhakaran MP, Zhang Y, Low S, Choon AT, Ramakrishna S. Biomimetic hydroxyapatite-containing composite nanofibrous substrates for bone tissue engineering. Philos Trans A Math Phys Eng Sci. 2010;368:2065–81.
39. Chen L, Wu Z, Zhou Y, Li L, Wang Y, Wang Z, et al. Biomimetic porous collagen/hydroxyapatite scaffold for bone tissue engineering. J Appl Polym Sci. 2017;134:45271.
40. Arun Kumar R, Sivashanmugam A, Deepthi S, Iseki S, Chennazhi KP, Nair SV, et al. Injectable chitin-poly(ε-caprolactone)/nanohydroxyapatite composite microgels prepared by simple regeneration technique for bone tissue engineering. ACS Appl Mater Interfaces. 2015;7:9399–409.
41. Ferraz MP, Monteiro FJ, Manuel CM. Hydroxyapatite nanoparticles: a review of preparation methodologies. J Appl Biomater Biomech. 2004;2:74–80.
42. Paz A, Guadarrama D, López M, González JE, Brizuela N, Aragón J. A comparative study of hydroxyapatite nanoparticles synthesized by different routes. Quim Nova. 2012;35:1724–7.
43. Salehi R, Hamishehkar H, Eskandani M, Mahkam M, Davaran S. Development of dual responsive nanocomposite for simultaneous delivery of anticancer drugs. J Drug Target. 2014;22:327–42.
44. Samiei M, Aghazadeh M, Movassaghpour AA, Fallah A, Aminabadi NA, Pakdel SMV, et al. Isolation and characterization of dental pulp stem cells from primary and permanent teeth. J Am Sci. 2013;9:153–7.
45. Zhang W, Yang N, Shi XM. Regulation of mesenchymal stem cell osteogenic differentiation by glucocorticoid-induced leucine zipper (GILZ). J Biol Chem. 2008;283:4723–9.
46. Stanford CM, Jacobson PA, Eanes ED, Lembke LA, Midura RJ. Rapidly forming apatitic mineral in an osteoblastic cell line (UMR 106-01 BSP). J Biol Chem. 1995;270:9420–8.
47. Azhar FF, Olad A, Salehi R. Fabrication and characterization of chitosan–gelatin/nanohydroxyapatite–polyaniline composite with potential application in tissue engineering scaffolds. Des Monomers Polym. 2014;17:654–67.
48. Mathew L, Narayanankutty SK. Synthesis, characterisation and performance of nanosilica as filler in natural rubber compounds. J Rubber Res. 2010;13:27–43.
49. Prabhakaran MP, Venugopal JR, Chyan TT, Hai LB, Chan CK, Lim AY, et al. Electrospun biocomposite nanofibrous scaffolds for neural tissue engineering. Tissue Eng Part A. 2008;14:1787–97.
50. Yang X, Chen X, Wang H. Acceleration of osteogenic differentiation of preosteoblastic cells by chitosan containing nanofibrous scaffolds. Biomacromolecules. 2009;10:2772–8.
51. Hong S, Kim G. Fabrication of electrospun polycaprolactone biocomposites reinforced with chitosan for the proliferation of mesenchymal stem cells. Carbohydr Polym. 2011;83:940–6.
52. Dinan B, Bhattarai N, Li Z, Zhang M. Characterization of chitosan based hybrid nanofiber scaffolds for tissue engineering. J Undergrad Res Bioeng. 2007;7:33–7.
53. Agrawal C, Ray RB. Biodegradable polymeric scaffolds for musculoskeletal tissue engineering. J Biomed Mater Res. 2001;55:141–50.
54. Salerno A, Fernández-Gutiérrez M, del Barrio JSR, Pascual CD. Macroporous and nanometre scale fibrous PLA and PLA–HA composite scaffolds fabricated by a bio safe strategy. RSC Adv. 2014;4:61491–502.
55. Rahman NA, Feisst V, Dickinson ME, Malmström J, Dunbar PR, Travas-Sejdic J. Functional polyaniline nanofibre mats for human adipose-derived stem cell proliferation and adhesion. Mater Chem Phys. 2013;138:333–41.
56. Gilbert PM, Havenstrite KL, Magnusson KE, Sacco A, Leonardi NA, Kraft P, et al. Substrate elasticity regulates skeletal muscle stem cell self-renewal in culture. Science. 2010;329:1078–81.
57. Raeisdasteh Hokmabad V, Davaran S, Ramazani A, Salehi R. Design and fabrication of porous biodegradable scaffolds: a strategy for tissue engineering. J Biomater Sci Polym Ed. 2017;28:1797–825.
58. Li Q, Chang Z, Oliveira G, Xiong M, Smith LM, Frey BL, et al. Protein turnover during in vitro tissue engineering. Biomaterials. 2016;81:104–13.
59. Chern MJ, Yang LY, Shen YK, Hung JH. 3D scaffold with PCL combined biomedical ceramic materials for bone tissue regeneration. Int J Precis Eng Manuf. 2013;14:2201–7.
60. Ganesh N, Jayakumar R, Koyakutty M, Mony U, Nair SV. Embedded silica nanoparticles in poly (caprolactone) nanofibrous scaffolds enhanced osteogenic potential for bone tissue engineering. Tissue Eng Part A. 2012;18:1867–81.
61. Li K, Sun H, Sui H, Zhang Y, Liang H, Wu X, et al. Composite mesoporous silica nanoparticle/chitosan nanofibers for bone tissue engineering. RSC Adv. 2015;5:17541–9.
62. Boskey AL. Biomineralization: conflicts, challenges, and opportunities. J Cell Biochem. 1998;72 Suppl 30–1:83–91.
63. Papagerakis P, Berdal A, Mesbah M, Peuchmaur M, Malaval L, Nydegger J, et al. Investigation of osteocalcin, osteonectin, and dentin sialophosphoprotein in developing human teeth. Bone. 2002;30:377–85.
64. Matsubara T, Kida K, Yamaguchi A, Hata K, Ichida F, Meguro H, et al. BMP2 regulates Osterix through Msx2 and Runx2 during osteoblast differentiation. J Biol Chem. 2008;283:29119–25.
65. Asghari F, Salehi R, Agazadeh M, Alizadeh E, Adibkia K, Samiei M, et al. The odontogenic differentiation of human dental pulp stem cells on hydroxyapatite-coated biodegradable nanofibrous scaffolds. Int J Polym Mater Polym Biomater. 2016;65:720–8.
66. Aghazadeh M, Samiei M, Alizadeh E, Porkar P, Bakhtiyari M, Salehi R. Towards osteogenic bioengineering of dental pulp stem induced by sodium fluoride on hydroxyapatite based biodegradable polymeric scaffold. Fibers Polym. 2017;18:1468–77.
67. Samiei M, Aghazadeh M, Alizadeh E, Aslaminabadi N, Davaran S, Shirazi S, et al. Osteogenic/odontogenic bioengineering with co-administration of simvastatin and hydroxyapatite on poly caprolactone based nanofibrous scaffold. Adv Pharm Bull. 2016;6:353–65.